PHYSICAL REVIEW B VOLUME 26, NUMBER 11 1 DECEMBER 1982

Monte Carlo studies of two-dimensional melting: Dislocation vector systems

Yukio Saito
Kernforschungsanlage Jülich GmbH, Institut für Festkörperforschung, 5170 Jülich, Federal Republic of Germany
(Received 18 May 1982)

Monte Carlo simulations of dislocation vector systems with long-range interactions reveal two possible types of phase transitions depending on the core energy of dislocations. For dislocations with a large core energy the melting transition is found to be continuous and due to dislocation unbinding. The Kosterlitz-Thouless theory agrees well with the simulation results. For a small core energy the melting transition is caused by the nucleation of grain boundary loops and is found to be first order. The latter transition may correspond to the previous computer experiments on various atomic systems. In addition to thermodynamic quantities such as the energy and specific heat, microscopic configurations and orientational correlation functions are also calculated.

I. INTRODUCTION

The Kosterlitz-Thouless (KT) renormalization-group method[1,2] has been very successful in describing phase transitions in various two-dimensional (2D) systems such as the magnetic phase transition of the 2D-XY model,[3–5] roughening transition of a crystal surface,[6–10] metal-insulator transition of a (logarithmic) Coulomb gas,[7–10] superfluid transition in two dimensions,[11,12] etc. The only exception is the melting transition of a 2D crystal. The KT theory[1,2] predicts a continuous phase transition caused by dislocation unbinding, and the extended theory by Halperin and Nelson[13,14] and Young[15] (HNY) predicts two successive continuous phase transitions due to dislocation and disclination unbinding. On the contrary, the existing molecular-dynamics or Monte Carlo simulations of atomic systems such as hard-core, soft-core, and Lennard-Jones systems, indicate a single melting transition which is first order with hysteresis.[16–20] For a Coulomb-gas[21–24] system the order of phase transition is still in dispute and no final agreement among various calculations is reached.

One possible cause of the discrepancy between theory and experiment is the shortness of the computation time or the smallness of the system sizes.[18] The other possibility is the inadequacy of the theoretical model. The renormalization-group theory calculates thermodynamic quantities of a continuous elastic medium with dislocations.[25] Compared to the atomistic models, there are many effects missing, for example, vacancies, anharmonicity, etc. If these neglected effects are essential, the dislocation model is insufficient to describe the melting transition. Another possibility has been pointed out by Chui[26] in a recent paper; he claims that the dislocation model is sufficient to describe the melting transition, but that the KT or HNY theory misses a possible collective excitation of dislocation vectors, namely grain boundaries.[24,25] He argues that for small core energy of dislocations, a first-order melting transition due to grain-boundary unbinding takes place before the continuous phase transition predicted by KT occurs.

Here are reported results of Monte Carlo simulations of dislocation vector systems, which have been reported briefly before.[27] The advantage of simulating the dislocation-vector system is that one can easily control the dislocation core energy. In fact, I have chosen two values of core energy E_c, and have found the melting transition to be first order for small E_c and continuous for large E_c. The continuous transition is due to the dislocation unbinding as predicted by KT, and the first-order melting transition seems to be due to nucleation of grain-boundary loops.

In the next section a model Hamiltonian of dislocation vectors is derived for a finite system with periodic boundary conditions. Section III describes the result of Monte Carlo simulations for a system with a large core energy, where the transition turns out to be continuous. Section IV describes the simulation results for a system with a small core energy, where the transition turns out to be first order. The last section summarizes the results and deals with the discussion on the mechanism of the first-order transition.

II. THE MODEL AND THE HAMILTONIAN

Monatomic systems with central forces may order in a close-packed crystal in the ground state, namely a triangular lattice in two dimensions. At finite temperatures dislocations[25] can be formed in the crystal. Assuming a_0 to be the lattice parameter of the triangular lattice, unit Burgers vectors can have six orientations; $\vec{B}=(\pm\vec{a_0},0)$ and $(\pm a_0/2, \pm\sqrt{3}a_0/2)$. Since an isolated dislocation costs energy proportional to the logarithm of the system size[25], Burgers vectors should satisfy the neutrality condition,

$$\sum_{I=1}^{N_B}\vec{B}_I=0\ , \tag{1}$$

where N_B is the total number of the dislocations. From continuum elasticity theory, the interaction between edge dislocations is found to be[25]

$$\mathscr{H}_0=-\frac{J}{2}\sum_{I\neq J}\sum\left[\vec{B}_I\vec{B}_J\ln\frac{R_{IJ}}{a}-\frac{(\vec{B}_I\cdot\vec{R}_{IJ})(\vec{B}_J\cdot\vec{R}_{IJ})}{R_{IJ}^2}\right]+E_c\sum_I\vec{B}_I^2\ , \tag{2}$$

where R_{IJ} is the distance between the Ith and Jth Burgers vectors, and the coupling constant J is given by the Lamé coefficients λ and μ as

$$J=\frac{\mu(\mu+\lambda)}{\pi(2\mu+\lambda)}\ . \tag{3}$$

a is a core radius of a dislocation and E_c is a core energy. On performing the Fourier transformation,

$$\vec{B}(\vec{q})=\sum_I^{N_B}\vec{B}_I e^{i\vec{q}\cdot\vec{R}_I}\ , \tag{4}$$

the Hamiltonian is rewritten as

$$\mathscr{H}_0=-\frac{J}{2}\int\frac{d^2\vec{q}}{(2\pi)^2}B^\alpha(\vec{q})B^\beta(-\vec{q})V^{\alpha\beta}(\vec{q})\ , \quad \alpha,\beta=x,y\ , \tag{5}$$

where the interaction $V^{\alpha\beta}(\vec{q})$ is given by

$$V^{\alpha\beta}(\vec{q})=\delta^{\alpha\beta}G(\vec{q})+U^{\alpha\beta}(\vec{q})\ . \tag{6}$$

Here $G(\vec{q})$ is the orientation-independent part and related to the Green's function q^{-2} as

$$G(\vec{q})=\frac{-2\pi}{q^2}-\ln a+\frac{2E_c}{J}-0.5\ , \tag{7}$$

and $U^{\alpha\beta}(\vec{q})$ represents the orientation-dependent part,

$$U^{\alpha\beta}(\vec{q})=-\frac{2\pi}{q^2}\left[\delta^{\alpha\beta}-\frac{2q^\alpha q^\beta}{q^2}\right]=\pi\left[\frac{\partial}{\partial q^\alpha}q^2\frac{\partial}{\partial q^\beta}\right]\frac{1}{q^2}\ . \tag{8}$$

In order to perform a computer simulation one has to consider a finite system in a rectangular box of size $\Omega=L_xL_y$ with periodic boundary conditions. I further assume that instead of the core radius a, dislocations are restricted to a triangular mesh point with a lattice parameter $2a$. The ith mesh site is represented as

$$\vec{r}_i=(x_i,y_i)=(la,\sqrt{3}ma)\ ,$$

where $0\le l<L=L_x/a$ and $0\le m<M=L_y/\sqrt{3}a$ with $l+m$ even. The total number of lattice points is $N=LM/2$. The wave vector $\vec{q}$ is correspondingly discretized

$$q_x=\frac{2\pi l}{La},\quad l=0,1,\ldots,L-1\ , \tag{9a}$$

$$q_y=\frac{2\pi m}{\sqrt{3}Ma},\quad m=0,1,\ldots,M-1\ . \tag{9b}$$

Accounting for the symmetry of the triangular lattice in the same way as done for the scalar Coulomb gas,[10] the Fourier-transformed Green's function in a continuous and infinite system, q^{-2}, in Eqs. (7) and (8), is now replaced by a triangular lattice Green's function,[28]

$$G_0(\vec{q})=\frac{6}{6-2\cos 2q_xa-2\cos(q_x+\sqrt{3}q_y)a-2\cos(q_x-\sqrt{3}q_y)a}\ . \tag{10}$$

The final form of the interaction Hamiltonian for a dislocation system on a triangular mesh of a finite size with periodic boundary conditions in x and y directions is written as

$$\mathscr{H}_N=-\frac{J}{2}\sum_{i\neq j}\sum b_i^\alpha b_j^\beta V_N^{\alpha\beta}(\vec{r}_i-\vec{r}_j)\ , \quad \alpha,\beta=x,y\ . \tag{11}$$

Here $\vec{b}_i$ represents a Burgers vector at the ith mesh site if it is occupied by a dislocation, and zero otherwise. The coupling $V_N^{\alpha\beta}(\vec{r})$ is given by

$$V_N^{\alpha\beta}(\vec{r})=\delta^{\alpha\beta}[G_N(\vec{r})+e]+U_N^{\alpha\beta}(\vec{r})\ . \tag{12}$$

Here e is constant related to the core energy, and

$$G_N(\vec{r})=\frac{2\pi}{\sqrt{3}LMa^2}\frac{1}{2}\sum_{q}{}''G_0(\vec{q})(1-e^{i\vec{q}\cdot\vec{r}}) \tag{13}$$

and

$$U_N^{\alpha\beta}(\vec{r})=\frac{\pi}{\sqrt{3}LMa^2}\frac{1}{2}\sum_{\vec{q}}{}''\left[\frac{\partial}{\partial q^\alpha}G_0^{-1}(\vec{q})\frac{\partial}{\partial q^\beta}G_0(\vec{q})\right]\times(1-e^{i\vec{q}\cdot\vec{r}})\ . \tag{14}$$

Since the lattice Green's function (10) becomes singular at two points (0,0) and $(\pi/a,\pi/\sqrt{3}a)$ and gives the same logarithmic contributions near these points, the two points are excluded from the $\vec{q}$ summation and a factor $\frac{1}{2}$ is introduced in front of the summation.

In the thermodynamic limit ($N\to\infty$) and a large separation $r\to\infty$, the orientation-independent interaction $G_N(\vec{r})$ asymptotically approaches a logarithmic form. This is shown in Fig. 1(a) for two system sizes, $L\times M=38\times22$ and 76×44, and $G_N(\vec{r})$ is approximated by

$$G_N(\vec{r})\sim\ln\frac{r}{a}+1.13\ . \tag{15}$$

The observed finite-size effect is very similar to the one for the scalar logarithmic Coulomb gas studied previously.[10] Figure 1(b) shows variations of orientation-dependent interactions along several directions. $U_N^{xx}(x,y)$ is well approximated by

$$U_N^{xx}(x,y)\sim-\frac{x^2-y^2}{2(x^2+y^2)}\ , \tag{16}$$

which is $\frac{1}{2}$ for $x=0$, $-\frac{1}{2}$ for $y=0$, and $\frac{1}{4}$ for $y=\sqrt{3}x$. The off-diagonal part $U_N^{xy}(x,y)$ is also approximated by

$$U_N^{xy}(x,y)\sim-\frac{xy}{x^2+y^2}\ , \tag{17}$$

which is 0 for $x=0$ or $y=0$, and $-\sqrt{3}/4$ for $y=\sqrt{3}x$. For large separations, however,

$$U_N^{xy}\left[\frac{r}{2},\frac{\sqrt{3}}{2}r\right]$$

deviates from the constant $-\sqrt{3}/4$ as shown in Fig. 1(b). This is due to the symmetry in the finite system,

$$U_N^{xy}(x,y)=-U_N^{xy}(L-x,y)=-U_N^{xy}(x,\sqrt{3}M-y)\ , \tag{18}$$

which forces

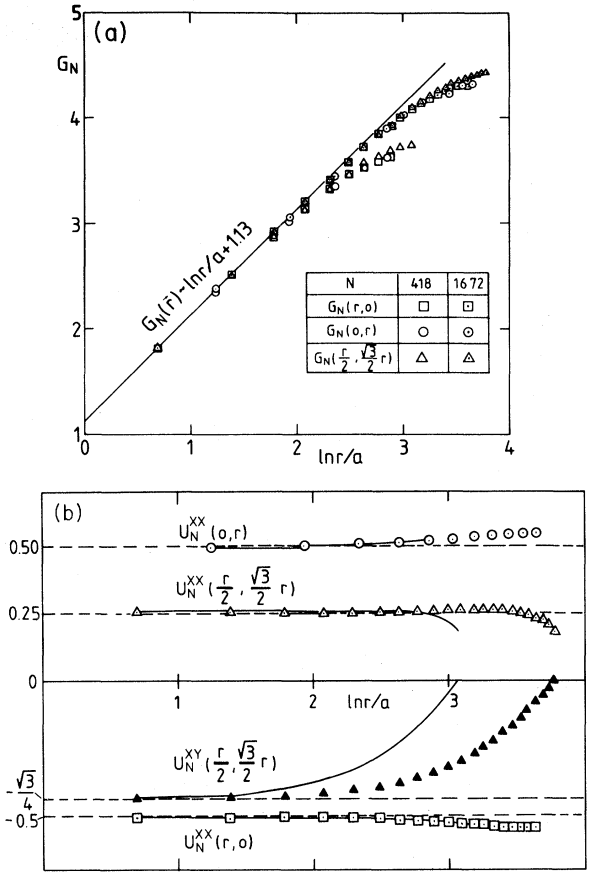

FIG. 1. (a) Orientation-independent interaction $G_N(r)$ of a finite system vs logarithm of the distance r. Two different sizes of the system, $N=418$ and 1672, and three different directions, $\vec{r}=(x,y)=(r,0)$, $(0,r)$, and $(r/2,\sqrt{3}r/2)$, are considered. (b) Orientation-dependent interaction $U_N^{xx}(r)$ and $U_N^{xy}(r)$ for the size $N=1672$. Dashed line represents the expected values for a system of infinite size. Continuous lines are the corresponding values for a system of small size, $N=418$.

$$U_N^{xy}\left[\frac{r}{2},\frac{\sqrt{3}}{2}r\right]$$

to vanish when r approaches L or M. Considering the asymptotic behavior [(15)–(17)] one sees that the Hamiltonian of a finite system (11) approaches the Hamiltonian (2) with a core energy

$$E_c=\frac{J}{2}(\tfrac{1}{2}+1.13+e)=\frac{J}{2}(1.63+e) \tag{19}$$

in the thermodynamic limit.

In order to illustrate that the Hamiltonian (11) contains the essential features of long-range interactions, let us calculate the energy density of a pair of grain boundaries.[24,26] We introduce two grain

boundaries parallel to the y axis with separation x in between. One grain boundary consists of stackings of dislocations with Burgers vector $(a_0,0)$ with separation s in the y direction, and the other with Burgers vector $(-a_0,0)$ with the same separation s. In an infinite and continuous system one can calculate the energy analytically from Eq. (2). The resulting energy density is[24,26]

$$\frac{\mathscr{H}}{2L_y/s}=\tfrac{1}{2}Ja_0^2\left[\ln\left[\frac{s}{\pi a}\sinh\frac{\pi x}{s}\right]-\frac{\pi x}{s}\coth\frac{\pi x}{s}\right]+E_c a_0^2 . \quad (20)$$

The first term on the right-hand side comes from the logarithmic interaction between dislocations and asymptotically produces energy cost proportional to the separation x. The orientation-dependent interaction between dislocations produces the second negative contribution in (20) which cancels the linear part of the first term. Consequently the energy density becomes asymptotically constant,

$$\frac{\mathscr{H}}{2L_y/s}\to\tfrac{1}{2}Ja_0^2\ln\frac{s}{\pi a}+E_c a_0^2 . \quad (21)$$

In our finite-size system with periodic boundary conditions, the corresponding energy density is shown by circles in Fig. 2. The horizontal axis $\exp[G_N(x,0)-1.13]$ is almost equal to x, and contains, furthermore, the size effect. Here the constant parameter e is chosen to be zero, or the core energy is $E_c\sim 0.82$ J. Since the separation between the dislocations in a grain boundary is $s=2\sqrt{3}a$ for a triangular mesh, we expect an asymptotic value of the energy density $\mathscr{H}/MJa_0^2\sim 0.52$ from Eq. (21), which agrees with the numerical result ~ 0.523 as shown in Fig. 2. If there is no orientation-dependent interaction U, the energy density is almost proportional to the separation x as shown by triangles in Fig. 2, and agrees well with the theoretical prediction for an infinite continuous system,

$$\mathscr{H}_{2L_y/s}\to\frac{\pi a}{2s}Ja_0^2x+\tfrac{1}{2}Ja_0^2\ln\frac{s}{\pi a}+E_c a_0^2 . \quad (22)$$

From these discussions we see that our model system with Hamiltonian (11)–(14) contains the essential features of the original system with Hamiltonian (2): the long-range logarithmic interaction and the orientation-dependent interaction characteristic to the vector system.

III. CONTINUOUS MELTING OF A SYSTEM WITH A LARGE CORE ENERGY

The procedure for the simulation of model Hamiltonian (11) is the following.[10,29] A pair of nearest-neighbor sites are chosen at random from the triangular mesh. If both sites are empty, a pair of dislocations with Burgers vectors opposite each other is tried to be created. If both sites are occupied by dislocations with Burgers vectors opposite each other, an annihilation of the pair is tried. Otherwise an exchange of sites is tried. The trial is accepted according to the Boltzmann weight; if the energy difference ΔE of the final state from the initial state is negative the configuration is changed, and if the difference ΔE is positive, the configuration is changed with the rate proportional to $e^{-\Delta E/T}$ at a temperature T. Here, and subsequently, the Boltzmann constant k_B is set to be unity. We have considered two system sizes, $L\times M=38\times 22$ and 76×44, the total number of mesh sites being $N=LM/2=418$ and 1672, respec-

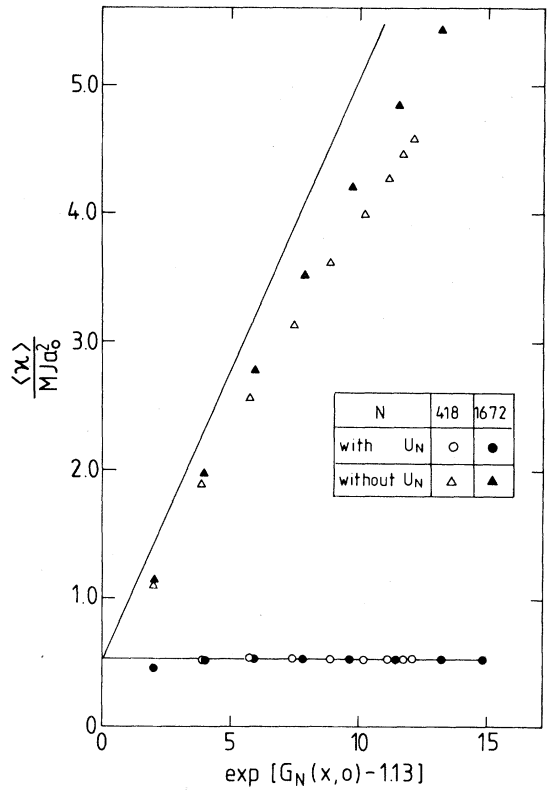

FIG. 2. Energy density of two grain boundaries $\langle\mathscr{H}_N\rangle/MJa_0^2$ as a function of their separation $\exp[G_N(x,0)-1.13]\sim x$. Circles represent values for the systems with orientation-dependent interaction U, and triangles without U. Closed symbols are for the larger system with $N=1672$ and the open symbols for the smaller system with $N=418$. Straight lines represent the analytical results, Eqs. (21) and (22), with $s=2\sqrt{3}a$ and $E_c=0.82$ J.

tively. These sizes are chosen such that $L_x = La \sim L_y = \sqrt{3}Ma$. 2000 to 4000 Monte Carlo steps (MCS) per nearest-neighbor bond (totally $3N$) are performed. Usually an initial 200 MCS are used for equilibrating the system. We have considered two cases with core energy $E_c = 0.82$ and 0.57 J. In this section the result of simulations with a large core onergy $E_c = 0.82$ J is described.

A. Energy and specific heat

First the thermodynamic quantities are considered in order to detect the phase transition. In Fig. 3 the average value of the energy per mesh sites

$$E = \frac{\langle \mathscr{H}_N \rangle}{NJa_0^2} , \tag{23}$$

and the specific heat per site,

$$c = \frac{(\langle \mathscr{H}_N^2 \rangle - \langle \mathscr{H}_N \rangle^2)}{NT^2} , \tag{24}$$

are shown as functions of the dimensionless temperature,

$$t = \frac{T}{Ja_0^2} . \tag{25}$$

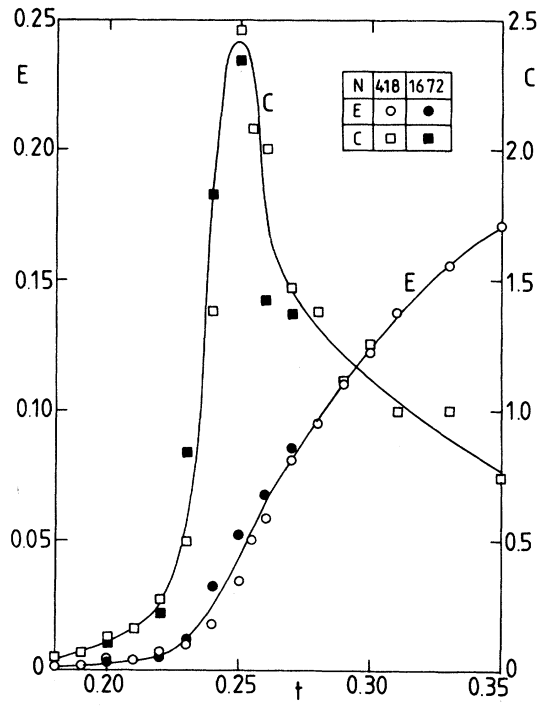

FIG. 3. Energy E and the specific heat c as a function of the reduced temperature t for systems with a larger core energy $E_c = 0.82$ J. Lines serve as a guide to the eye.

No discontinuity or hysteresis are found in the energy. The specific heat has a rather sharp maximum at a temperature $t \sim 0.25$. The peak height seems to be independent of the system size, but due to the large fluctuations around the maximum height, it is difficult to decide whether the peak is that of the second-order phase transition or whether it merely represents the enhanced short-range order as the case of the KT continuous transition.[1-3]

B. Microscopic configuration and the dislocation density

In order to identify phases of the system, we now look at the microscopic configuration of dislocation vectors. Figure 4 shows snapshot configurations at various temperatures for the smaller system with $N = 418$. For $t = 0.20$ in Fig. 4(a) only very few dislocations are created and almost all of them are tightly bounded. At $t = 0.30$ in Fig. 4(d) many dislocations are present and some of them are isolated. The formation of these unbound dislocations are taking place between $t = 0.22 \sim 0.25$ [Figs. 4(b) and 4(c)]. Similar behavior is also found for the larger system with $N = 1672$. As for the quantitative analysis, the average density of dislocations n for each type of Burgers vectors is shown in Fig. 5. At low temperatures the density follows the Arrhenius law,

$$n = n_0 e^{-\Delta E/t} , \tag{26}$$

with the activation energy $\Delta E \sim 1.50$, which is near the minimum formation energy $\Delta E \sim 1.30$ of a nearest-neighbor pair of dislocations. For $t \geq 0.22$ the density of dislocation increases more than the value expected from Eq. (26). The excess density seems to correspond to that of free and unbound dislocations. At still higher temperatures the density saturates because the total density of dislocations, $6n$, becomes of the order of 0.5.

C. Renormalized coupling and shear modulus

In the preceding section it turned out that the phase transition seems to be induced from the unbinding of the dislocation pairs, just as predicted by KT. Since more predictions for the quantative features of the phase transition are given, we now calculate and compare those quantities, namely the renormalized coupling constant K_R and the shear modulus.[1,2,13-15]

The Lamé coefficients are renormalized by the

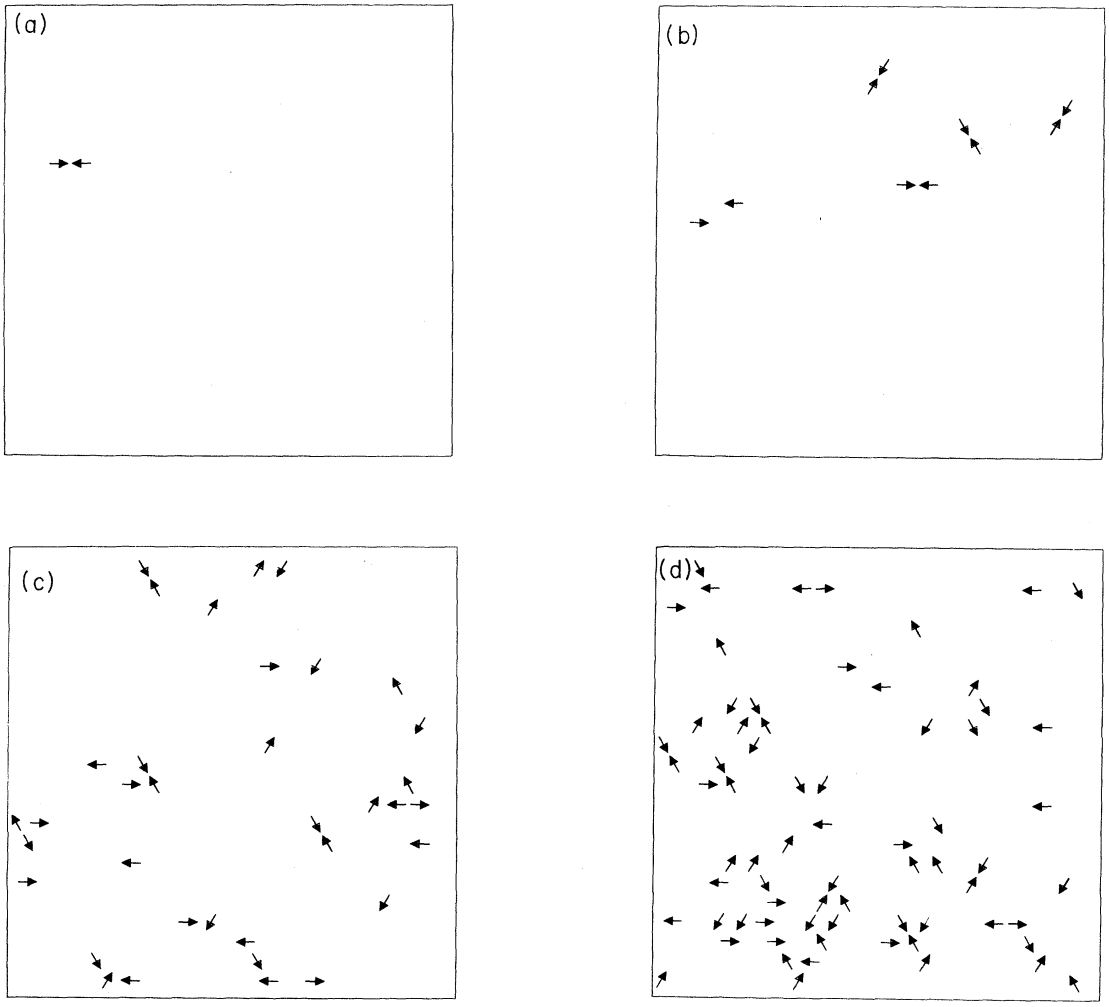

FIG. 4. Snapshot configurations of dislocation vectors in a small system. Temperatures are (a) $t=0.20$, (b) 0.22, (c) 0.25, and (d) 0.30, respectively.

dislocations, and according to Halperin and Nelson,[14] the renormalized Lamé coefficients λ_R and μ_R are related to the correlation function by

$$C^{-1}_{R,\alpha\beta\gamma\delta}=C^{-1}_{\alpha\beta\gamma\delta}+\frac{\langle U^{\rm sing}_{\alpha\beta}U^{\rm sing}_{\gamma\delta}\rangle}{Na_0^2}$$
$$=\frac{T}{4\mu_R a_0^2}(\delta_{\alpha\gamma}\delta_{\beta\delta}+\delta_{\alpha\delta}\delta_{\beta\gamma})$$
$$-\frac{T\lambda_R}{4\mu_R(\mu_R+\lambda_R)a_0^2}\delta_{\alpha\beta}\delta_{\gamma\delta}\ , \qquad (27)$$

where $\alpha,\beta,\gamma,\delta$ represent the components x or y. The elastic term is given by the bare and nonrenormalized Lamé coefficients λ and μ as

$$C^{-1}_{\alpha\beta\gamma\delta}=\frac{T}{4\mu a_0^2}(\delta_{\alpha\gamma}\delta_{\beta\delta}+\delta_{\alpha\delta}\delta_{\beta\gamma})$$
$$-\frac{T\lambda}{4\mu(\mu+\lambda)a_0^2}\delta_{\alpha\beta}\delta_{\gamma\delta}\ , \qquad (28)$$

and the quantity $U^{\rm sing}$ represents a dislocation contribution

$$U^{\rm sing}_{\alpha\beta}=\tfrac{1}{2}\sum_i(b_i^\alpha\epsilon^{\beta\gamma}r_i^\gamma+b_i^\beta\epsilon^{\alpha\gamma}r_i^\gamma)\ , \qquad (29)$$

where $\epsilon^{xy}=1=-\epsilon^{yx}$ and zero otherwise. Since the simulations are done for a finite system with mesh structure and with periodic boundary conditions, I modify the above expression by replacing x_i and y_i by

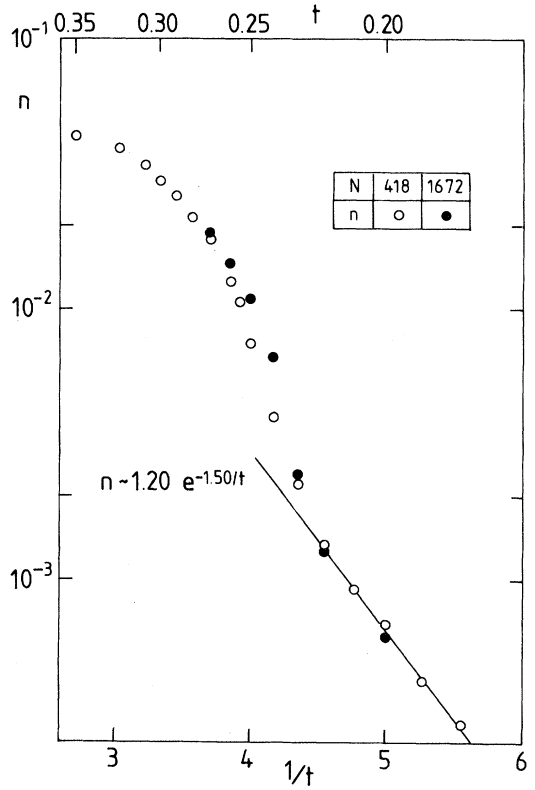

FIG. 5. Dislocation density n as a function of the inverse temperature $1/t$. Straight line at low temperatures describes the Arrhenius law with an activation energy $\Delta E = 1.50$, corresponding to the formation of bound pairs.

$$x_i \to \frac{L_x}{2\pi} \sin\frac{2\pi}{L_x} x_i \ , \qquad y_i \to \frac{L_y}{2\pi} \sin\frac{2\pi}{L_y} y_i \ . \tag{30}$$

From Eq. (27) the renormalized coupling constant K_R is defined by

$$K_R^{-1} \equiv \frac{T(2\mu_R + \lambda_R)}{4\mu_R(\mu_R + \lambda_R)a_0^2} = C^{-1}_{R,\alpha\alpha\alpha\alpha} = K^{-1} + \frac{\langle U^{\rm sing}_{\alpha\alpha} U^{\rm sing}_{\alpha\alpha} \rangle}{N a_0^2} \ . \tag{31}$$

Here $C_{R,\alpha\alpha\alpha\alpha}$ means $xxxx$ or $yyyy$ component, and the elastic contribution is given by

$$K = \frac{4\pi J a_0^2}{T} = \frac{4\pi}{t} \ . \tag{32}$$

In the KT theory K_R is expected to be finite at low temperatures and to decrease with increasing the temperature, taking the universal value 16π at

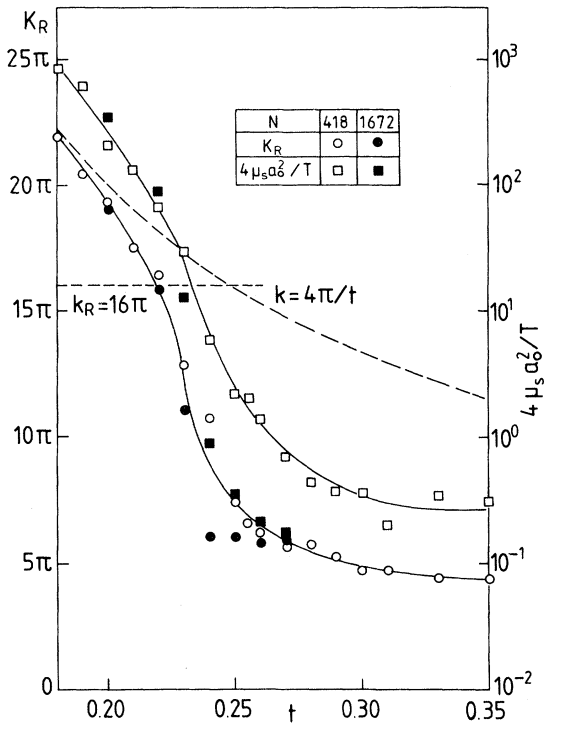

FIG. 6. Renormalized coupling K_R and the singular part of the shear modulus μ_s. μ_s are shown in the logarithmic scale.

the transition temperature, and vanishing above the transition temperature. Figure 6 shows K_R obtained by Monte Carlo simulations as a function of t. At low temperatures where there are few dislocations K_R is almost equal to the bare value K shown by the dashed line, whereas at high temperatures the deviation of K_R from K becomes large. The deviation takes place around $t \sim 0.22$, where K_R takes the value about 16π. The transition point $t \sim 0.22$ agrees with that obtained from the dislocation density, and the value of K_R agrees well with the universal value predicted by the KT theory. Our K_R in the high-temperature phase remains finite. This may be due to the finiteness of our system size, because the fluctuation $\langle U^{\rm sing} U^{\rm sing} \rangle$ can only diverge in the thermodynamic limit. We now estimate the renormalized shear modulus μ_R, which is related to the correlation $C_{R,xyxy}$ by

$$C^{-1}_{R,xyxy} = C^{-1}_{R,yxyx} = \frac{T}{4\mu_R a_0^2} = \frac{T}{4\mu a_0^2} + \frac{\langle U^{\rm sing}_{xy} U^{\rm sing}_{xy} \rangle}{N a_0^2} \ . \tag{33}$$

However, since the bare Lamé coefficient μ is not known in our system, we can only calculate the singular part of the shear modulus μ_s defined by

$$\mu_s^{-1}=\frac{4}{NT}\langle U_{xy}^{\text{sing}}U_{xy}^{\text{sing}}\rangle \ . \tag{34}$$

This is related to the renormalized shear modulus by

$$\mu_s=\frac{\mu\mu_R}{\mu-\mu_R} \ .$$

In Fig. 6, $4\mu_s a_0^2/T$ is shown in logarithmic scale, and one finds a rapid decrease of μ_s near $t\sim 0.22$. This agrees with the prediction by KT theory that the shear modulus vanishes when the dislocations unbind.

D. Orientational correlation

Until now every result seems to fit well to the KT theory. According to Halperin and Nelson[13,14] (HN), however, the high-temperature phase is not the true liquid phase, since isolated dislocations cannot destroy the orientational order completely. Taking $\theta(r)$ to be the orientation relative to some fixed reference axis of the bond between two neighboring atoms, they have concluded that the correlation function,

$$C_\theta(\vec{r})=\langle[\theta(\vec{r})-\theta(\vec{0})]^2\rangle \ , \tag{35}$$

behaves logarithmically for large separation r at temperatures higher than the KT transition temperature. In other words, the correlation of the order parameter of bond orientations,

$$\langle\psi_6(r)\psi_6(0)\rangle=\langle e^{6i[\theta(r)-\theta(0)]}\rangle \ , \tag{36}$$

decays to zero, but only algebraically, indicating an enhanced orientation order. They therefore called the phase "hexatic." In this section we calculate the contribution of dislocations to the orientational correlation function. The orientation due to Burgers vectors are derived by Halperin and Nelson[14] in the Fourier transformed space as

$$\theta_s(\vec{q})=\frac{-i\vec{q}\cdot\vec{b}(\vec{q})}{q^2} \ . \tag{37}$$

Taking the effects of finite-size and the periodic boundary conditions, the singular part of the orientational correlation function can be expressed as

$$C_\theta^s(\vec{r})\equiv\langle[\theta_s(\vec{r})-\theta_s(\vec{0})]^2\rangle=\frac{1}{LMa^2}\sum_{\vec{q}}{}''\langle b^\alpha(\vec{q})b^\beta(\vec{q})^*\rangle\left[\frac{1}{2}\frac{\partial}{\partial q^\alpha}G_0^{-1}(\vec{q})\frac{\partial}{\partial q^\beta}G_0(\vec{q})+\delta^{\alpha\beta}G_0(\vec{q})\right] \ . \tag{38}$$

Figure 7 shows $C_\theta^s(x,0)$ obtained by Monte Carlo simulations for various temperatures. The horizontal axis $G_N(x,0)$ is asymptotically equal to $\ln x$, and it furthermore contains the finite-size effect.[10] At low temperatures, C_θ^s remains constant asymptotically, whereas at high temperatures it is almost proportional to G_N or $\ln x$. This confirms that the high-temperature phase here is the hexatic phase.

Another related quantity is the following correlation function:

$$\frac{T}{K_A(\vec{q})}=\frac{\langle[\vec{q}\cdot\vec{b}(\vec{q})][\vec{q}\cdot\vec{b}(-\vec{q})]\rangle}{q^2MLa^2} \ . \tag{39}$$

The long-wavelength limit of $K_A(\vec{q})$ is the orientational stiffness constant K_A, which corresponds to the slope of the orientational correlation $C_\theta^S(\vec{r})$ against $\ln r$. In the solid phase K_A is infinite, in the liquid phase zero; only in the hexatic phase is K_A finite and nonvanishing. The wave-vector dependence of the correlation function $T/K_A(q)$ averaged in x and $y=\sqrt{3}x$ directions is shown in Fig. 8. The long-wavelength limit of $T/K_A(q)$ seems to be vanishing for $t\lesssim 0.23$, and remains finite for $t\gtrsim 0.24$. Thus the solid-hexatic phase transition around $t=0.22-0.23$ is again confirmed. The HN theory predicts a hexatic-liquid phase transition due to the disclination unbinding at the point where $T/K_A=\pi/72$. From Fig. 8 that corresponds to the temperature around $t\sim 0.27$. However, we cannot investigate the second melting transition from the hexatic phase to the true liquid phase without orientational order, since disclinations are not considered here.[13,14,30]

IV. FIRST-ORDER MELTING TRANSITION OF A SYSTEM WITH A SMALL CORE ENERGY

In the preceding section the melting transition is found to be induced by the unbinding of dislocation pairs and the formation of free dislocations, as is predicted by KT. However, since the KT theory is based on the fugacity ($\sim e^{-E_c/T}$) expansion, it may be possible that the theory breaks down at small core energy and allows new phenomena to take place. Here we consider the system with a small core energy $E_c=0.57$ J, corresponding to $e=-0.5$. The simulation procedures are the same as those in the preceding section.

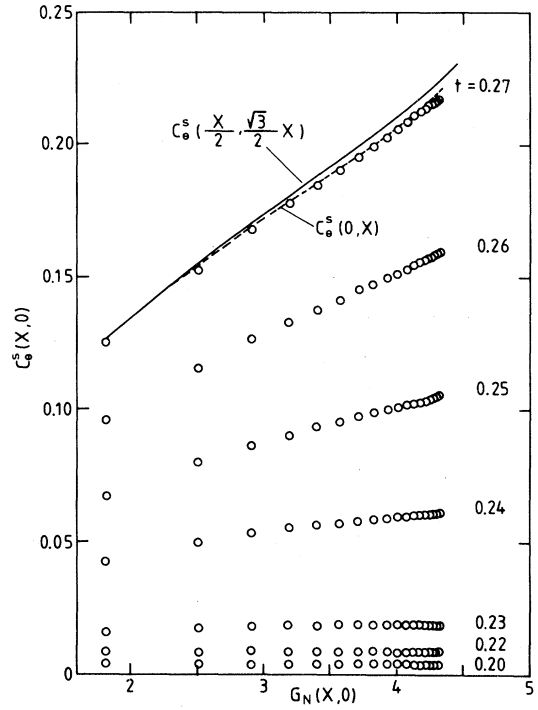

FIG. 7. Orientation-correlation function in the x direction $C_\theta^s(x,0)$ vs $G_N(x,0)$, which is almost proportional to $\ln x$. Continuous and broken lines represent C_θ^s vs G_N in $(0,x)$ and $(x/2,\sqrt{3}/2x)$ directions at $t=0.27$.

A. Energy and specific heat

The energy and the specific heat are shown in Fig. 9. One now sees a clear discontinuity and hysteresis in the energy, indicating a first-order transition. On heating the crystal phase where there are no dislocations, the lower branch of the E-t curve is obtained. At $t=0.14$ the lower branch becomes unstable and jumps up to the upper E-t branch. On cooling back, the upper branch stays stable and hysteresis is observed. The states at $t=0.13$ and 0.12 are metastable with a large fluctuation in the energy, as is shown by vertical bars for the smaller system in Fig. 9. The specific heat has a discontinuity at the transition point $t=0.14$. The specific heat in the metastable states depends on the system size, and becomes as large as about 4.0 for the smaller system.

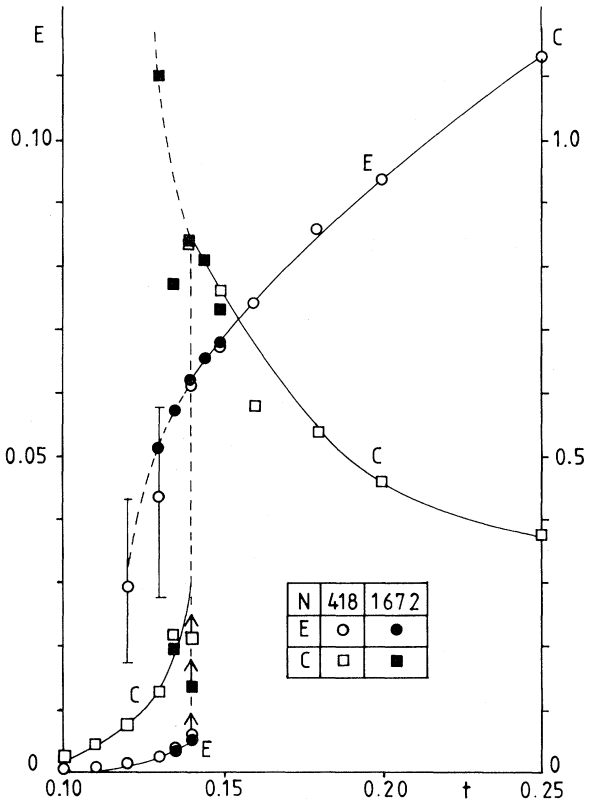

FIG. 9. Energy E and the specific heat c for the systems with small core energy $E_c=0.57$ J. Straight lines are just a guide for the eyes.

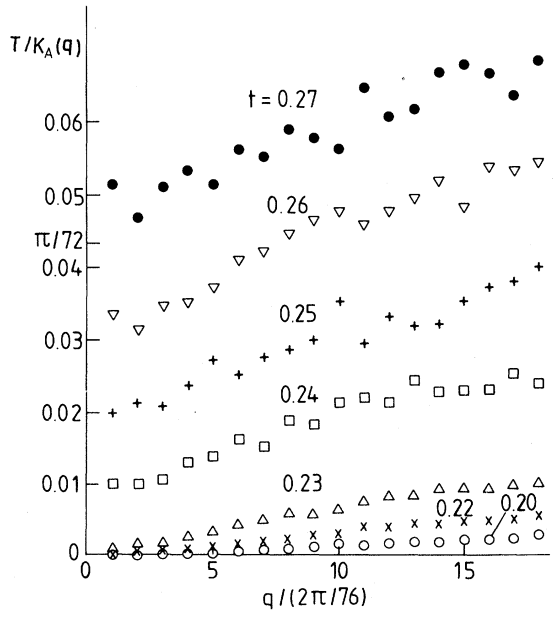

FIG. 8. Correlation function $T/K_A(q)$ of Eq. (39) vs q.

B. Microscopic configurations and the dislocation density

The phases are easily characterized by looking at the microscopic configurations directly. Snapshot configurations of dislocation vectors at various temperatures for the larger system are shown in Fig. 10. At $t=0.135$ on the lower E-t branch only a few

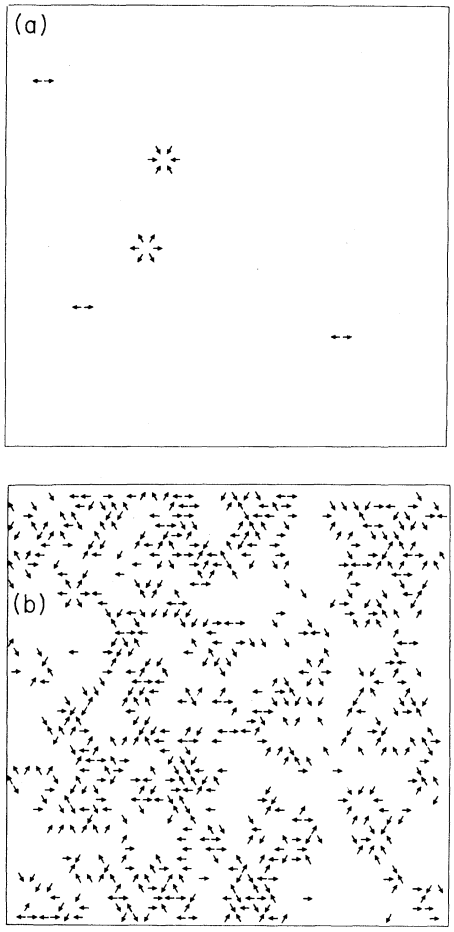

FIG. 10. Snapshot configurations of dislocation vectors in a large system, $N=1672$. Temperatures are (a) $t=0.135$ and (b) 0.145.

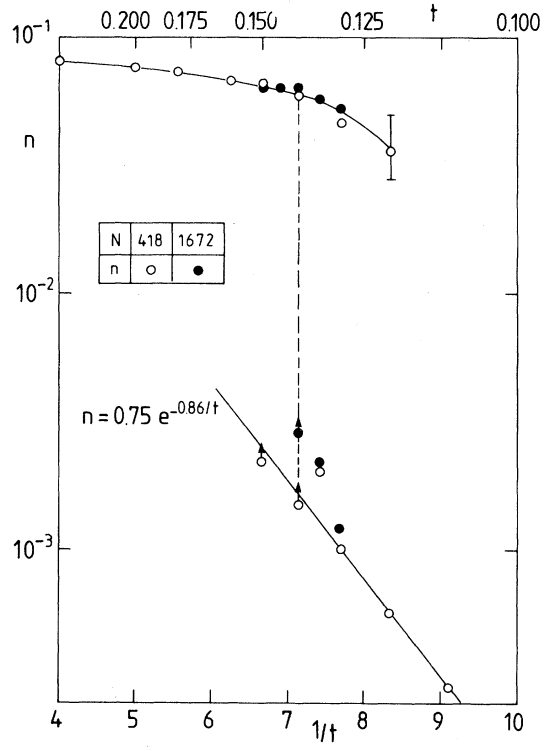

FIG. 11. Dislocation density n as a function of the inverse temperature $1/t$. Arrhenius law is shown by a straight line with an activation energy $\Delta E \sim 0.86$, corresponding to the formation of bound pairs.

dislocations are found as shown in Fig. 10(a) and most of them form bound pairs, quite similar to the solid-phase configurations in Figs. 4(a) and 4(b). One difference here is that one sometimes sees loops of dislocation vectors created and annihilated. In fact, at high temperature, $t=0.145$ in Fig. 10(b), one finds many dislocations, most of whom seem to form clusters or loops. There are not so many isolated dislocations as in Fig. 4(d).

The loops of dislocations are entangled and folded, and extend through the whole system, and thus may destroy the orientational order of the crystal globally. Therefore, the high-temperature phase may be called as true liquid. We will come back to this aspect later.

Corresponding to the first-order phase transition, the dislocation density now has a large discontinuity and hysteresis as is shown in Fig. 11. At low temperatures the density fits the Arrhenius law as before with the activation energy now $\Delta E \sim 0.86$, which is near the minimum of the pair-formation energy 0.80. At high temperatures, on the contrary, the density is very large and shows very weak temperature dependence, indicating that saturation is reached.

C. Renormalized coupling and shear modulus

The renormalized coupling K_R and the singular part of the shear modulus μ_s have been calculated and are shown in Fig. 12. The smallness of μ_s at high temperatures supports the identification of the high-temperature phase as liquid. The renormalized coupling K_R decreases on increasing the temperature and shows a discontinuity at $t=0.14$. The value $K_R \sim 23\pi$ at $t=0.14$ is still larger than the value 16π predicted by KT, indicating that the first-order transition has taken place before the KT continuous phase transition occurs. This has been also found in the previous molecular-dynamics experiments.[20]

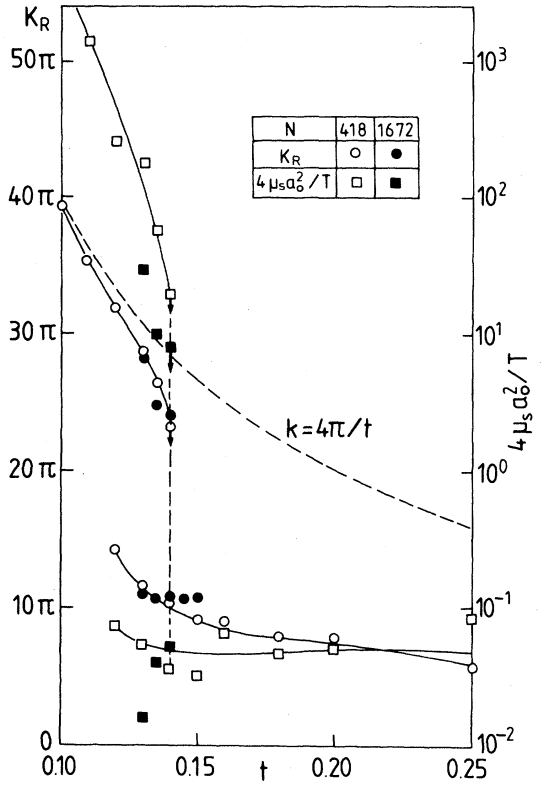

FIG. 12. Renormalized coupling constant K_R and singular part of the shear modulus μ_s.

D. Orientational correlation

As mentioned in Sec. IV B, the extended loops of dislocations may destroy the orientational order completely. This effect can be seen in the orientation-correlation function $C_\theta^s(r)$ which is shown in Fig. 13. In the crystal phase at $t=0.13$ the correlation function saturates at a small value. In the liquid phase, although C_θ^s shows some orientation dependence probably due to the slow relaxation of grain-boundary loop conformations, $C_\theta^s(x,0)$ increases faster than $G(x,0)$ (which is approximately proportional to $\ln x$). The correlation of the bond orientation $\langle \psi_6(\vec{r})\psi_6(\vec{0})\rangle$ may thus decay faster than the power law, and the system is not in the hexatic phase but the true liquid phase. The correlation function $T/K_A(q)$ defined by Eq. (39) shows a drastic change of behavior on varying the temperature as is shown in Fig. 14. Below $t<0.14$ correlation function is small and vanishes in a long-wavelength limit ($q\to 0$), indicating that the system is in a solid phase. Above $t\geq 0.14$, where the system melts and the density of dislocations becomes quite large, $T/K_A(q)$ becomes also quite large and it seems to increase in a long-wavelength

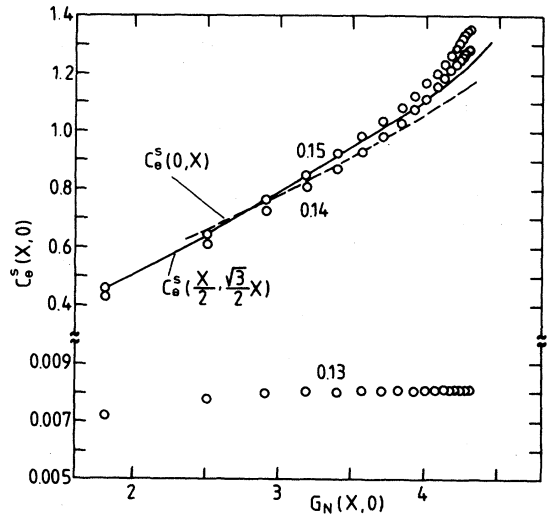

FIG. 13. Orientation-correlation function in the x direction $C_\theta^s(x,0)$. Continuous and broken lines represent C_θ^s vs G_N in $(0,x)$ and $(\frac{1}{2}x,\sqrt{3}/2x)$ directions at $t=0.15$.

limit. Albeit the large fluctuations and orientation dependence, the orientational stiffness K_A defined as a long-wavelength limit of $K_A(q)$ clearly satisfies the condition $T/K_A > \pi/72$ to form a true liquid

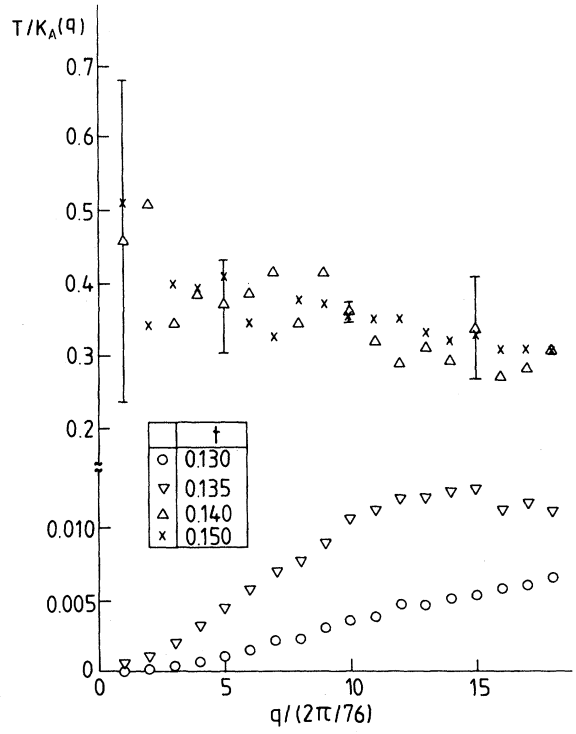

FIG. 14. Correlation function $T/K_A(q)$ vs q. Vertical bars denote fluctuations of the data due to the orientation dependence.

without orientational order.[14] Thus one can conclude that the observed first-order phase transition is a melting from the solid to the true liquid phase.

E. Kinetics of phase transition

From the investigations of the static and thermodynamic quantities in previous sections, the melting transition of a system with a small core energy is found to be first order. Now we consider the kinetic aspects of the phase transition.

Sequences of snapshot configurations of the melting crystal at $t=0.14$ for the small system are shown in Fig. 15. On starting from the perfect crystal with no dislocations, the system remains in a crystal phase until 1100 MCS. Then the clusters of dislocations begin to form. Some smallest loops, as is shown near the right-hand edge in Figs. 15(a) and 15(b), remain stable, but a larger loop on the left-hand lower corner grows in size [Fig. 15(b) at 1400 MCS], coalesces with the smaller loops [Fig. 15(c) at 1500 MCS], and finally covers the whole space. We can see this final stage more clearly for the larger system ($N=1672$). Small loops nucleated at the upper left-hand corner in Fig. 16(a) at 700 MCS grow [Fig. 16(b) at 900 MCS] and eat into the crystal region in the lower right-hand corner [Fig. 16(c) at 1100 MCS]. The melting takes place homogeneously and every site is a possible nucleation center, but when it starts nucleating, melting proceeds fast and further nucleation centers cannot be found in our small systems.

On cooling the liquid below the melting temperature $t=0.14$, the number of dislocations decreases a little but the system does not reach the equilibrium solid phase. By looking at dislocation configurations of supercooled liquid at $t=0.13$ shown in Fig.

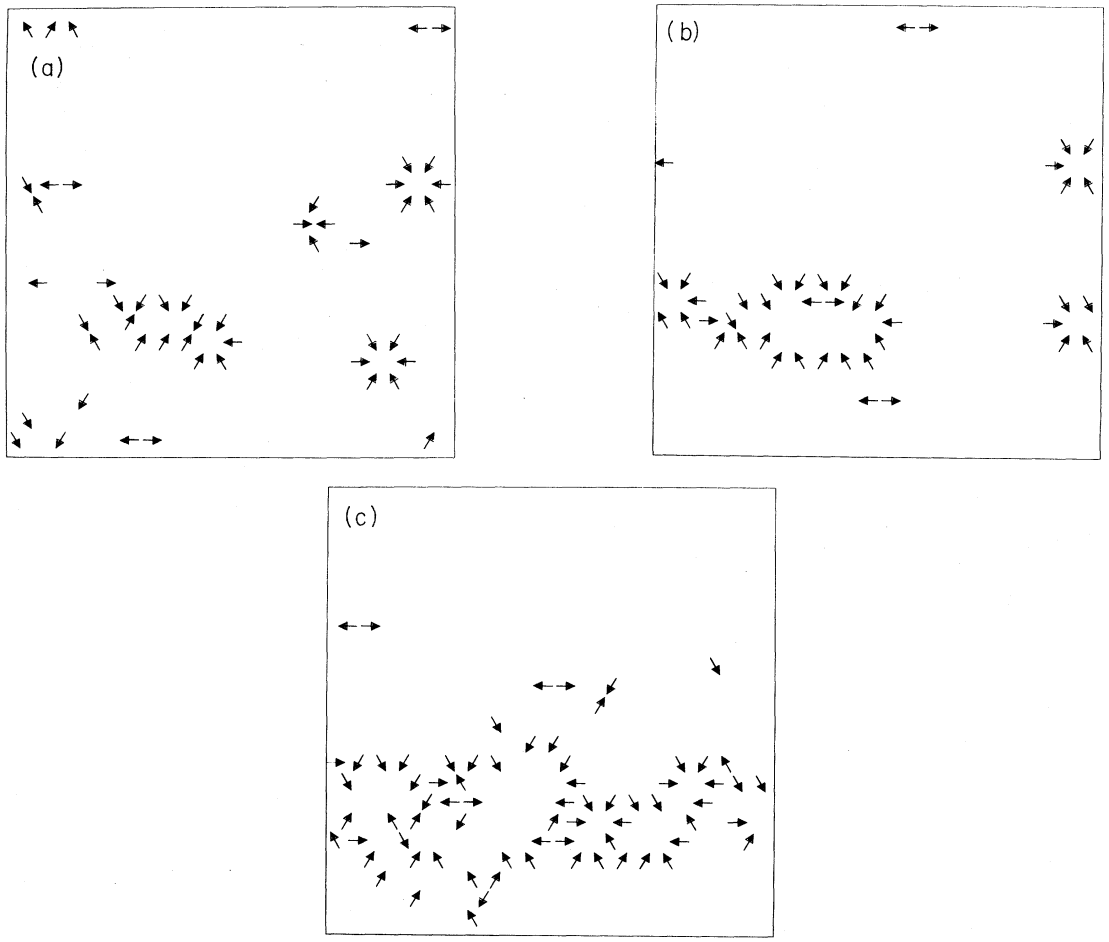

FIG. 15. Melting process of a crystal in the small system $N=418$ at the temperature $t=0.14$. Time sequences are (a) 1300 MCS, (b) 1400 MCS, and (c) 1500 MCS.

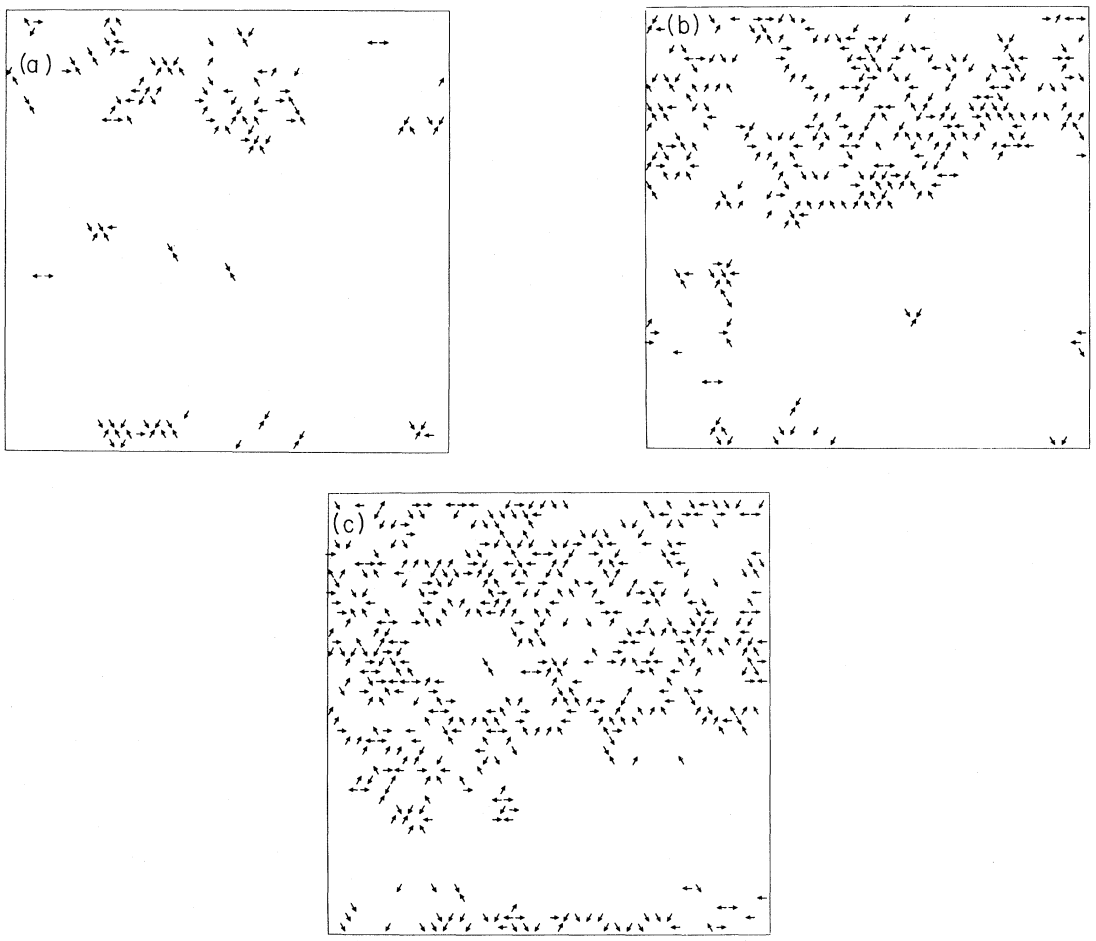

FIG. 16. Melting process of a crystal in the large system $N=1672$ at the temperature $t=0.14$. Time sequences are (a) 700 MCS, (b) 900 MCS, and (c) 1100 MCS.

17 one finds that some of the dislocation vectors form a closed loop of dislocations [Fig. 17(a)] or extended grain boundaries [Fig. 17(b)], which stay metastable. Therefore, the system cannot relax to the equilibrium crystal phase within our limited computation time.

V. CONCLUSIONS AND DISCUSSIONS

From Monte Carlo simulations on dislocation-vector systems with a logarithmic orientation-independent interaction and a long-ranged orientation-dependent interaction, two types of melting transition are found to be possible: a continuous melting for a large core energy and a first-order melting for a small core energy. The continuous transition is due to the dislocation unbinding, and is well described by the KT renormalization-group theory. The transition temperature, for example, is characterized by the renormalized coupling $K_R=16\pi$. The first-order transition is due to the nucleation of grain-boundary loops and the transition takes place at K_R larger than 16π, or in other words, before the KT transition takes place. This first-order transition may correspond to that found in the previous molecular-dynamics and Monte Carlo simulations of various atomistic systems, since similar loops of dislocation vectors are also found in atomic systems.[18]

A qualitative explanation of the grain-boundary-loop nucleation may be the following: As is found in Eq. (21) the energy density of a grain boundary is asymptotically constant, and thus the energy E of a grain boundary with length l can be approximately given to be proportional to the length l. On the other hand, for a grain boundary in a system with coordination number z, there are approximately $(z-1)^l$ possible conformations for a loop. Therefore, the entropy S also turns out to be proportional

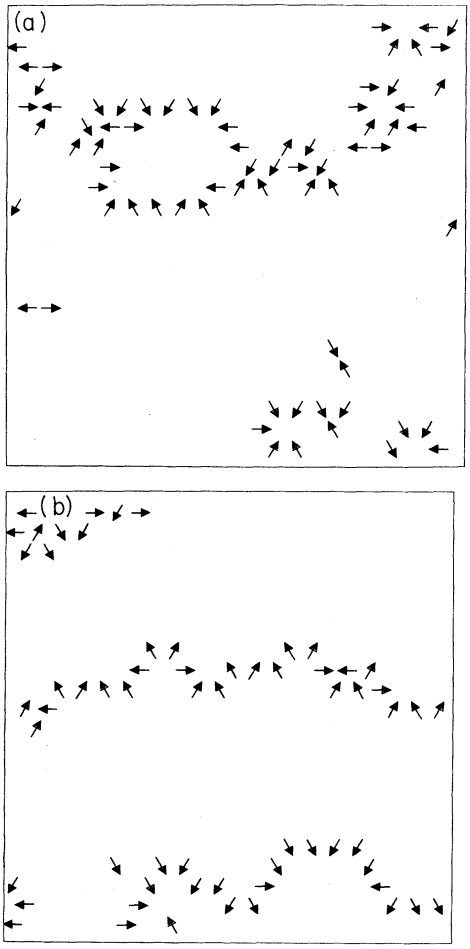

FIG. 17. Configuration of supercooled liquid at $t=0.13$ in the small system $N=418$. Times are (a) 800 MCS and (b) 1400 MCS.

to the length l. Since the free energy is given by $F=E-TS$, one expects l to be zero at low temperatures to minimize the energy, and l to be infinite at high temperatures in order to gain the entropy. Although this may qualitatively explain the first-order melting transition, more detailed quantitative investigations including many-body effects are necessary.

Upon varying core energy one finds a change in the character of phase transition. This implies the existence of a critical core energy where the phase transition changes from first order to the continuous one. From our simulation results the critical core energy should be between 0.82 and 0.57 J. In order to determine the critical core energy more precisely, more elaborate methods such as the real-space renormalization-group method or Monte Carlo renormalization-group calculations may be useful. As for the calculation of the core energy in the atomic models there is only one calculation in the one-component plasma.[24] The value obtained $E_c \sim 1.22$ J seems to support a continuous phase transition, whereas there are still some disputes and no final agreement on the order of phase transition reached. The calculation of the core energies for other atomic systems therefore seems to be urgent.

Finally I comment on the system size. The simulations are done for a system of rather small size, N. However, from the previous investigation of the Coulomb-gas system[10] similar to our system, the continuous KT transition has been well characterized even in small systems, unless one investigates the precise position of the transition temperature or its critical phenomena. When the system performs a first-order transition in our system, grain-boundary loops are found to be nucleated with a small critical radius. Thus our system size is sufficient to detect the change of melting mechanism from the KT theory. The size effect, for example, shown in Fig. 11 does not affect the mechanism of melting, and probably may not change the nature and order of the transition.

ACKNOWLEDGMENTS

Acknowledgments are due Professor H. Müller-Krumbhaar for discussions and a reading of the manuscript. Also acknowledged are participants of the Centre Européen des Calculs Atomiques et Moléculaires (CECAM) workshop held in Orsay, France, where the work was motivated.

[1]J. M. Kosterlitz and D. J. Thouless, J. Phys. C 6, 1181 (1973).
[2]J. M. Kosterlitz, J. Phys. C 7, 1046 (1974).
[3]J. V. José, L. P. Kadanoff, S. Kirkpatrick, and D. R. Nelson, Phys. Rev. B 16, 1217 (1977).
[4]J. Tobochnik and G. V. Chester, Phys. Rev. B 20, 3761 (1979).
[5]S. Miyashita, H. Nishimori, A. Kuroda, and M. Suzuki, Prog. Theor. Phys. 60, 1669 (1978).
[6]H. J. F. Knops, Phys. Rev. Lett. 39, 766 (1977).
[7]S. T. Chui and J. D. Weeks, Phys. Rev. B 14, 4978 (1976).
[8]T. Ohta and K. Kawasaki, Prog. Theor. Phys. 60, 365 (1978).

[9]R. H. Swendsen, Phys. Rev. B 18, 492 (1978).
[10]Y. Saito and H. Müller-Krumbhaar, Phys. Rev. B 23, 308 (1981).
[11]D. R. Nelson and J. M. Kosterlitz, Phys. Rev. Lett. 39, 1201 (1977).
[12]V. Ambegaokar, B. I. Halperin, D. R. Nelson, and F. D. Siggia, Phys. Rev. Lett. 40, 783 (1978).
[13]B. I. Halperin and D. R. Nelson, Phys. Rev. Lett. 41, 121 (1978).
[14]D. R. Nelson and B. I. Halperin, Phys. Rev. B 19, 2457 (1979).
[15]A. P. Young, Phys. Rev. B 18, 1855 (1979).
[16]D. Frenkel and J. P. McTague, Phys. Rev. Lett. 42, 1632 (1979).
[17]F. F. Abraham, Phys. Rev. Lett. 44, 463 (1980).
[18]S. Toxvaerd, Phys. Rev. Lett. 44, 1002 (1980); Phys. Rev. A 24, 2735 (1981).
[19]E. van Swol, L. V. Woodcock, and J. N. Cape, J. Chem. Phys. 73, 913 (1980).
[20]F. F. Abraham, in *Ordering in Two Dimensions,* edited by K. Sinha (North-Holland, Amsterdam, 1980).
[21]R. W. Hockney and T. R. Brown, J. Phys. C 8, 1813 (1975).
[22]R. C. Gann, S. Chakravarty, and G. V. Chester, Phys. Rev. B 20, 326 (1979).
[23]R. H. Morf, Phys. Rev. Lett. 43, 931 (1979).
[24]D. S. Fisher, B. I. Halperin, and R. H. Morf, Phys. Rev. B 20, 4692 (1979).
[25]F. R. N. Nabarro, *Theory of Dislocations* (Clarendon, Oxford, 1967).
[26]S. T. Chui, Phys. Rev. Lett. 48, 933 (1982).
[27]Y. Saito, Phys. Rev. Lett. 48, 1114 (1982).
[28]If one uses a square mesh, the square-lattice Green's function

$$G_{0,\mathrm{sq}}=\frac{1}{(4-2\cos q_x a-2\cos q_x a)}$$

should be used instead of the triangular lattice one. Here a is the lattice parameter of the square mesh. From the preliminary calculations the main results of our work do not seem to change if one uses the square mesh.
[29]See, for example, *Monte Carlo Calculations in Statistical Physics,* edited by K. Binder (Springer, Heidelberg, 1979).
[30]D. R. Nelson (unpublished).